Evaluation of a Cesium-Ion Rocket Employing a Large Porous Tungsten Ionizer

R. J. CYBULSKI* AND J. T. KOTNIK†
NASA Lewis Research Center, Cleveland, Ohio

An ion-rocket engine has been operated for more than 50 hr using a porous tungsten ionizer. The ionizer was assembled using the techniques of electron-beam welding combined with a high-temperature furnace braze. Accelerator and power efficiencies of 90% and 70%, respectively, were obtained at a current density of 113 amp/m^2. This power efficiency was obtained at a specific impulse of 8680 sec. Preliminary results indicate a propellant-utilization efficiency of about 90%.

Introduction

THIS work is part of a continuing program to develop an ion rocket that could some day be used for space propulsion. There are two objectives to be reported which were pursued in this work. First it is desirable to develop an ion rocket with the highest possible thrust density. It is necessary therefore to keep the ionizer surface as large as possible compared to the total frontal area. Secondly, it is desirable to maintain a high power efficiency, which means that the current density should be as high as possible with the power losses minimized. With these goals in mind it was undertaken to fabricate large porous tungsten ionizers.

One of the major problems connected with the use of porous tungsten as an ionizer has been the difficulty encountered in the fabrication and joining of the ionizer. The joining poses serious problems. The joint must not leak, the high work function of the porous tungsten must be preserved, and no weldment can be allowed to run over the ionizer surface resulting in a filling or blocking of the pores. The materials used for joining should have low vapor pressures so that evaporation of the weldment will not create local high pressure regions that might cause electrical breakdown in the engine. The ionizers must be operated at temperatures in excess of 1370°K, without further sintering of the material.

Many techniques for joining porous tungsten have been tried. Examples are brazing with several braze materials, resistance welding, arc welding, arc spraying, and electron-beam welding. These techniques are discussed in Ref. 1.

Several sizes and shapes of porous tungsten ionizers have been tried. The first type reported in Ref. 1 used $\frac{1}{4}$-in.-diam porous tungsten plugs. Another type reported[2] employs a porous tungsten annular ring with a mean diameter of 3 in.

The porous ionizer to be discussed herein was fabricated completely out of refractory metals. The technique used to join these metals was electron-beam welding. This method will be described in a later section.

To substantiate the feasibility of electron-beam welded porous tungsten ionizers, the performance of such an electrostatic ion rocket engine with a 6-in.-long by 0.3-in.-wide ionizer is reported.

Apparatus

This section of the report will describe the design development of a porous tungsten ionizer from the state previously reported in Ref. 3 as well as the instrumentation and apparatus with the actual tests.

Vacuum chamber

The data reported herein were obtained from experiments conducted in one of the high-vacuum electric-rocket research facilities at the Lewis Research Center. The vacuum facility is discussed fully in Ref. 4. The engine is mounted entirely from an aluminum endplate (see Fig. 1), which inserts into a 14-in.-long metal bell jar. The engine chamber is separated from the main portion of the vacuum facility by a 12-in.-diam pneumatically operated gate valve. Adjustments and changes in the engine could be made quickly

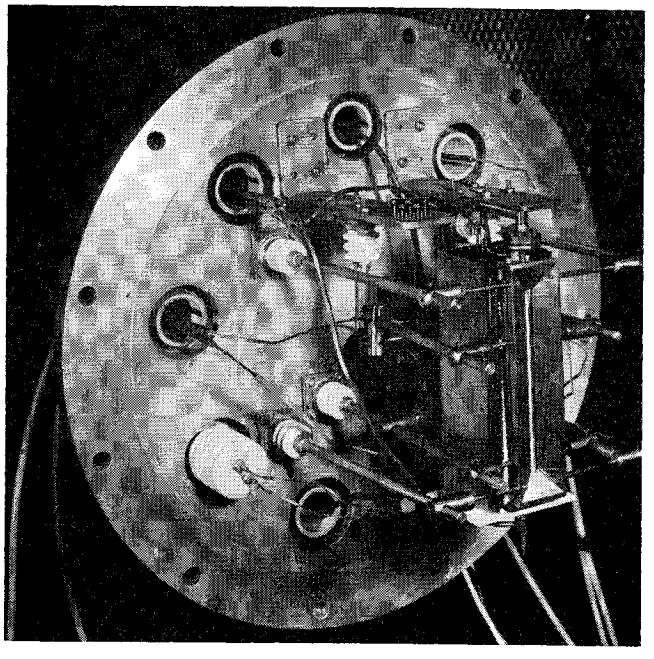

Fig. 1 Photo of engine on endplate

and conveniently by closing the valve between the bell jar and the tank; in this way the vacuum in the tank could be maintained continuously. The pressure in the engine chamber and main portion of the facility was maintained in the low 10^{-6} torr range while the engine was operating.

Ion engine

The engine was a modified version of the porous tungsten cesium-ion engine reported in Ref. 3. The disassembled engine is shown in Fig. 2a.

Cesium propellant is contained in a stainless-steel vaporizer located behind the porous tungsten ionizer. The cesium

---

Presented at the ARS Electric Propulsion Conference, Berkeley, Calif., March 14–16, 1962.

* Physicist (General), Aerospace Research Engineer. Associate Fellow Member AIAA.

† Physicist (General), Aerospace Research Engineer. Member AIAA.

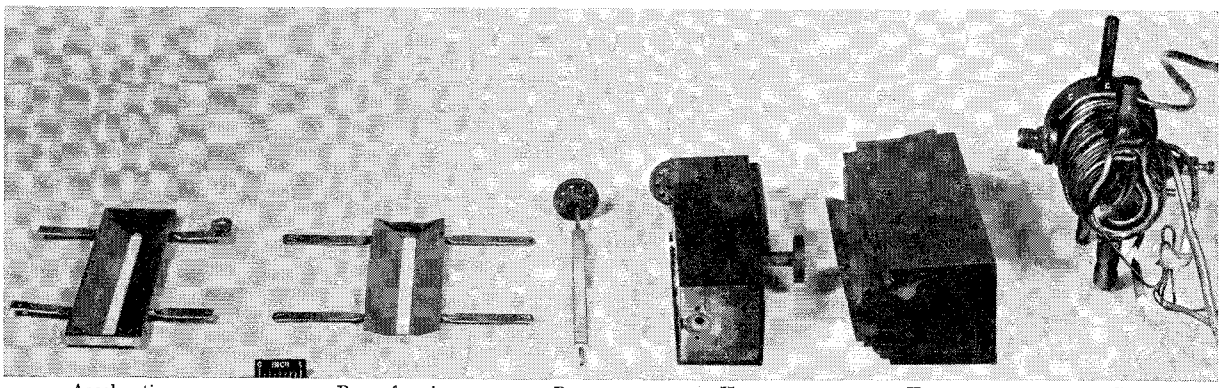

Fig. 2a Ion engine components

vapor passes through a $\frac{1}{4}$-in.-diam tantalum tube, which is flanged to a $\frac{1}{8}$-in.-diam tantalum tube, and into a reservoir behind the ionizer. The cesium vapor then passes through the porous tungsten and is ionized. Cesium ions created at the ionizer are accelerated by an electrostatic field maintained between the ionizer and the accelerator electrode. A beam-forming electrode maintained at the same potential as the ionizer is located at the downstream surface of the ionizer. Its purpose is to contain the ion beam within the prescribed boundaries. The accelerating electrode is maintained at a potential equal to or less than a negative 3 kv in order to prevent backstreaming of electrons.

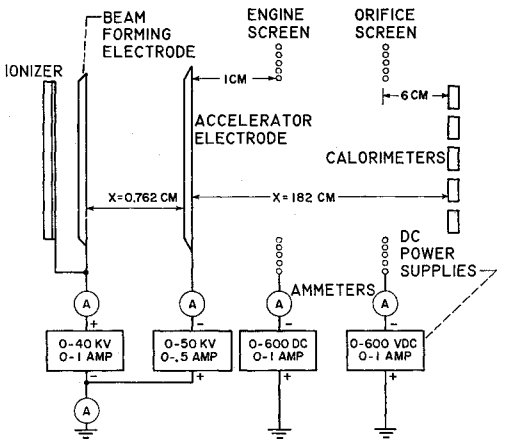

Fig. 2b Ion engine electrical schematic

The schematic shown in Fig. 2b gives the location of the power supplies and current meters used to monitor engine performance. All electrical leads, thermocouples, and air cooling connections are brought through aluminum oxide standoffs mounted on the endplate (see Fig. 1). An engine isolation screen maintained at a negative 300 v is located just downstream of the accelerator electrode. The screen prevents secondary electrons created in the test environment from reaching the engine. Such an electron flow would cause the ground return meter to indicate erroneously high beam currents.

Instrumentation

Electrical meters

All the meters used in this research are conventional commercial meters with $\pm 3\%$ of full scale accuracy. Net ion-beam powers, accelerator power losses, power input to ionizer, and vaporizer powers were calculated from the observed meter readings.

Conventional calorimeter

A complete discussion of the development of this instrument can be found in Ref. 5. The calorimeter is movable in a direction transverse to the ion beam. The measured readings of each of the 5 calorimeters in the array, at each position, then can be summed up and the total power obtained can be compared to the power obtained from the meter readings.

Vaporizer Design

The vaporizer was constructed of stainless steel, cylindrical in shape, 2 in. in diameter and 4.38 in. in length with a removable top to facilitate cesium loading. For a more complete description see Ref. 6. An iron-constantan thermocouple, located at the coldest portion of the vaporizer, was used to monitor propellant flow rate that is a function of vaporizer temperature.

Ionizer Design

As mentioned earlier, the purpose of this program was to develop an efficient porous tungsten ionizer and propellant system. The initial attempt at using a strip porous tungsten ionizer has been reported in Ref. 3. Initially, the porous tungsten ionizer was held in place by a mechanical clamping arrangement. This method proved undesirable because of excessive conduction heat losses through the beam-forming electrode and leakage of propellant around the ionizer. The power input required to heat this ionizer was 1.20×10^6 w/m^2 at 1370°K. Subsequent methods were pursued in an attempt to find an ionizer design that met the following requirements: 1) simplicity of design, 2) freedom from leaks around the porous ionizer, 3) durability, and 4) high heating efficiency.

The successful unit with which the data included in this paper were obtained consisted of a 0.3-in.- by 6-in.- by 0.050-in.-thick porous tungsten ionizer electron beam welded to a 6-in.-long 0.010-in.-wall tungsten channel. This arrangement is shown in Fig. 2a. The ends of the channel were then closed by furnace brazing. The propellant supply tube entered from the end of the channel. The porous ionizer was heated by radiation and conduction from the back wall of the channel, which was heated by radiation from a 0.005- × 0.31- × 6-in. tantalum heater filament. The power required was 1.51×10^5 w/m^2 at 1370°K.

The ionizer channel was mounted inside a five-sided box to facilitate heat shielding. The function of the box was to add structural rigidity to the channel and to hold in place the heat shielding. Connections for engine mounting were made at points where the temperature was low, thereby minimizing conduction losses. The assembled engine is shown in Fig. 1. This arrangement allowed removal of the

engine from the vacuum facility by simply removing four bolts that held the aluminum endplate to the metal bell jar.

Ionizer Construction

The construction of a leak tight, efficiently heated emitter was accomplished by using a U-shaped channel made from 0.010-in. tungsten. A channel is formed with an inside width of 0.304 in. and a depth of 0.150 in. The channel and porous tungsten then are jigged in the electron-beam welder to weld the long seam. A 3-ma electron beam at 120 kv then is passed perpendicular to the porous tungsten surface over the seam at a speed of 5 in./min. The beam then melts both the solid tungsten and porous tungsten, although the 0.010 sheet tungsten melts faster. The unit then is placed in an electron disintegrater machine, and the slightly oversized porous tungsten ends are burned off to exactly the length of the channels, 6 in. End pieces, slightly larger than the cross section of the tube, are made out of solid tungsten and holes in the center are burned out by the electron disintegrater machine. The end pieces and the channel unit then are jigged in the electron-beam welder and the seam between the solid tungsten end pieces and the porous tungsten are then sealed with a beam of the same power level just mentioned.

The unit then is removed from the welding jig, and a $\frac{1}{8}$-i.d. tantalum tube is placed into the holes in the endplates, and a brazing mixture is applied to the three open seams on the endplate and around the tube joint. The braze material, which melts at 3800°F, consists of 50% molybdenum powder, 40% molybdenum boride (MoB_2), and 10% titanium hydride (TiH_2). The unit with the brazing mixture applied then is brazed in a vacuum atmosphere at a pressure of 2μ.

The tube on one end of the unit then is crimped and heliarced closed and is used as a support for the bottom of the emitter. The longer tube at the top has a flange attached to it and is the feed tube for the cesium vapor.

Electrode Design

A complete summary of the electrode design used herein has been presented in Ref. 6 and therefore will be described only briefly herein. A paraxial ion beam is assumed to exist, and Poisson's equation is solved to obtain the potential distribution along the beam edge. Using this potential distribution and the boundary condition of zero electric field strength normal to the beam edge, Laplace's equation then is solved in the charge-free region outside the beam.

This solution determines the equipotential shapes outside the desired beam. If metal electrodes shaped to conform to these equipotential are maintained at the proper voltages and distances relative to the ion source, the ion beam, in theory, can be confined to the desired region. In practice, aperture effects and the necessity of using a finite number of electrodes will result in some departure from the assumed paraxial beam.

Results and Discussion

Propellant-Utilization Efficiency

One test has been run with this ionizer and propellant-feed system in an attempt to measure the propellant-utilization efficiency, η_u. This was done by running for a fixed period of time at a constant operating condition. The amount of cesium remaining then was determined by chemical analysis. Subtracting this from the original amount of cesium and dividing it by the run time yields the average mass flow rate. Converting this value of mass flow into its equivalent current and dividing it into the ion current delivered by the engine would yield η_u. The experimental value obtained in this manner was $\eta_u = 0.9\ (\pm 3\%)$.

Two possibilities of error were present in this method. The first is the failure to remove all of the unused propellant from the vaporizer and feed system before the chemical analysis. The second possibility is that there could have been a very small leak in the propellant feed system. The problem of intermittent leaks in the flange connecting the ionizer assembly to vaporizer has been observed since the construction of the leak tight ionizer, and several methods of sealing the system presently are being investigated. Both of these problems could make the observed value of propellant-utilization efficiency lower than the actual value.

Ionizer Power Consumption

The major energy loss of an ion rocket engine is the power required to heat the ionizer. Therefore independent heat shielding tests were conducted in order to determine the effect of various combinations of heat shielding on the reduction of power input to the ionizer as read on conventional meters.

In these heat shielding tests, the ionizer was mounted in a manner similar to but not the same as that used in the actual engine. In addition the beam-forming and accelerator electrodes were not present. Figure 3 compares the various heat-shielding schemes. The power input to the ionizer as indicated by conventional meters is shown as a function of the observed ionizer temperature. Initially the ionizer was operated without any tantalum heat-shielding, and the necessary data were obtained. Then a single heat shield was placed round the three sides of the channel and the run repeated. Multiple heat shields with 6, 16, and 27 heat shields were tested and because the power consumption was only slightly better for the 27 shields than for the 6 and 16 shields, only data for the 27 heat shields is shown. The final run presented is with the 27 heat shields and a strip of insulation added between the edge of the channel and the first heat shield. The power required for this configuration was 2.9×10^5 w/m^2 at 1370°K. The dashed curve (E) is for the actual heat-shielding configuration used to obtain the engine performance data presented herein. The major part of the difference in power input between curves D and E after accounting for the difference in conduction heat losses from the two mounting arrangements can be attributed to the effectiveness of the accelerator electrodes as heat shields. It has been measured experimentally that, of the 170-w difference in power between curves D and E at 1370°K, 30 w can be charged to conduction heat losses, and the remaining 140 w were due to heat-shielding effects of the electrodes. The ratio of radiation power loss with electrodes to power without, for an accelerating length to width ratio of one, is numerically equal to 0.55. If the electrodes served as perfect heat shields for an accelerating length to aperture width ratio of one, this value would be 0.41 as discussed in Ref. 7.

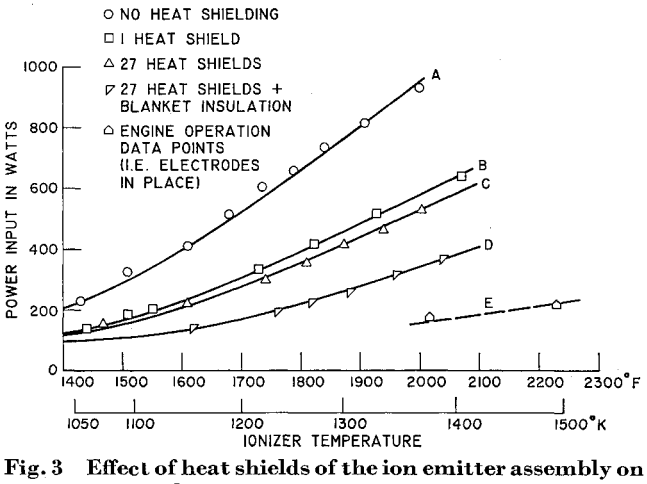

Fig. 3 Effect of heat shields of the ion emitter assembly on heater power requirements

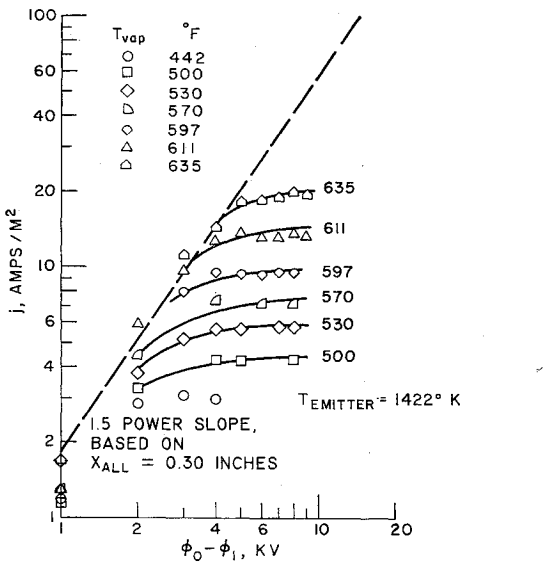

Fig. 4 Current densities as a function of accelerator potential compared to the current density calculated from Child's Law

These data show that the electrodes do serve as reasonably good heat shields. The resultant power to heat the ionizer to 1370°K with the complete engine assembly is 1.51×10^5 w/m².

Ion-Beam Current Density

The following sections will deal with engine performance. Beam, accelerator, and radiation power will be based on electrical measurements.

Figure 4 compares the current densities obtained by Child's law for space-charge limited flow as a function of accelerating potential for an accelerating distance of 0.3 in. These data fall reasonably close to Child's law.

Several causes can be mentioned as to why these data do not follow Child's law exactly:

1) Patch effect. Any emitter can exhibit small variations of work function over its surface, so that some portions will reach saturation at lower values of potential than others. The result will be a rounding off of the curve as demonstrated in these data of Fig. 4.

2) The effect of nonuniform emitter temperature. In operation the emitter temperature is not uniform (due to end cooling by conduction); the cooler portions will reach emission saturation before the hotter portions, and there will be a progressive deviation from the theoretical space-charge line in the region where saturation is approached.

Current densities as high as 113 amp/m² have been operated for periods of time up to 10 min, while current densities up to 80 amp/m² have been continuously operated up to 1½ hr without bringing out any major engine shortcomings such as a structural failure of emitter.

Porosity of Porous Emitter

The porous tungsten used in this program was obtained from Semicon Associates Company in the form of slabs measuring 6 in. by 0.3 in. by 0.050 in. Cold flow tests showed the transmission coefficient to be 4.5×10^{-5} (ratio of flow through the porous emitter to the flow that would obtain in an equal-area duct with no restriction). Figure 5 shows a photomicrograph of a portion of this same porous ionizer. The average pore size of the ionizer as measured from the photomicrograph is 2.5 to 3.0 μ. Reference 8 discussed the theory of atom loss from a porous tungsten ionizer as a function of pore size and ionizer temperature. Using the theory in Ref. 5 for an ionizer temperature of 1500°K (approximately the range operated) and summing the total losses from surface diffusion and vapor-phase flow, a total percent loss of 3 to 4% is obtained. This value compares reasonably well with the propellant-utilization efficiency of 0.9 mentioned earlier.

Accelerator Efficiency

One of the most important parameters which must be maximized in order to operate an ion engine efficiently is the accelerator efficiency η_{acc}. The accelerator efficiency is defined as the ratio of the beam power to the sum of the beam power and the power intercepted at the accelerating electrode. The term efficiency may be misleading, since the electrode erosion resulting from impingement is more serious than the power loss. If an ion engine is to be of use for long term operation, the ion impingement must be so low that the accelerator efficiency is essentially 100%.

For the data reported herein, η_{acc} varied from 80 to 97%. It is felt that two causes may have contributed to the rather high impingement currents on the accelerating electrode. First, the longitudinal weld between the channel and the porous tungsten ionizer caused the unit to warp in the longitudinal direction so that the center of the ionizer was $\frac{1}{16}$ in. back from the beam-forming electrode, as shown in Fig. 6. This could result in initially poor focusing of the ion beam. Second, the aperture area in the accelerator was 5% less than the ionizer surface area. Assuming a paraxial ion beam uniformly distributed over the ionizer surface, 5% of the beam would strike the accelerator electrode directly. Secondary electron emission from the accelerator electrode should result in electrode currents well above those due to ion arrival.

Power Efficiency

Figure 7 shows data of power efficiency η_p against specific impulse I_{sp} at constant-current density. Two curves of experimental data are shown. The lower curve, for a current density of 40 amp/m², has power efficiency up to 51%

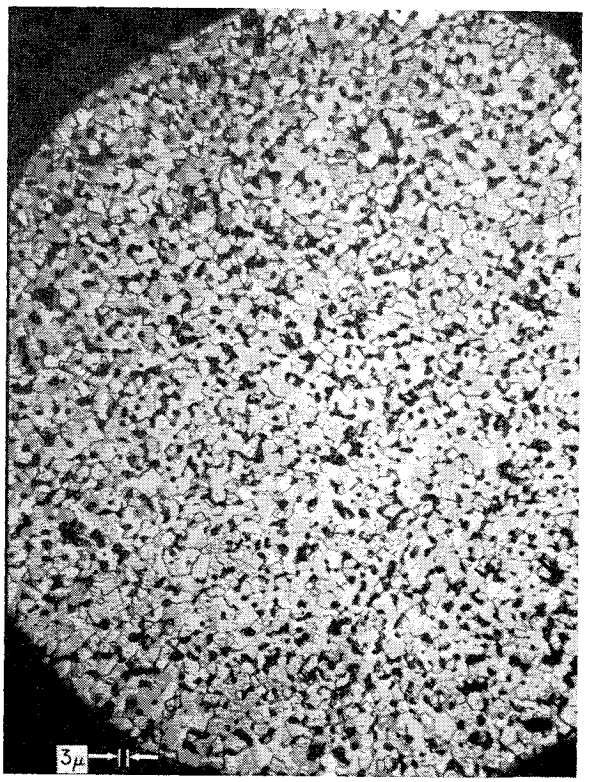

Fig. 5 Photomicrograph of porous tungsten used in this experiment; measured average pore diameter 2.5 to 3.0 μ

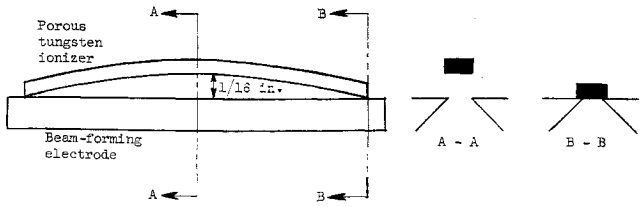

Fig. 6 Diagram of ionizer warping in the longitudinal direction due to heating during fabrication

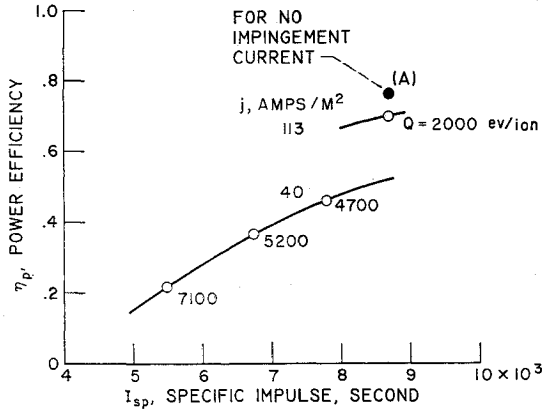

Fig. 7 Power efficiencies of porous tungsten ionizer obtained with current densities of 40 amp/m² and 113 amp/m², ϕ_{acc}/ϕ_{net} = 2/1 except I_{sp} = 5500 when ϕ_{acc}/ϕ_{net} = 2½/1

at a specific impulse of 8500 sec which corresponds to 4400 ev/ion. The upper curve consisting of only one data point operated at a current density of 113 amp/m² shows a power efficiency of 70% at a specific impulse of 8680 sec which corresponds to 2000 ev/ion. For this point, 5% of the ionizer current impinged on the accelerating electrode. If it is assumed that the impingement current can be eliminated a power efficiency of 76.5% is obtained. This number is depicted by point A in the figure.

Figure 8 compares the performance of an electron bombardment ion engine,[9] an annular porous tungsten engine,[2] a small diameter button porous tungsten engine,[10] and the porous tungsten engine reported herein. For the purposes of this comparison two slightly different parameters are introduced. These are the effective specific impulse I_{eff} and the rocket efficiency η_R, as derived in Ref. 7.

These data indicate that for effective specific impulses of less than 8000 sec, the electron-bombardment engine will be superior to the type of ion-rocket engine discussed in this report unless current densities of the order of 200 amp/m² are obtained or until the heat losses to the ionizer are reduced further. However, for effective specific impulses of more than 8000 sec the two engines compare rather well.

The upper curve (Fig. 8) derived in Ref. 7 for an emissivity based on polished tungsten depicts the theoretical values of rocket efficiency which can be obtained as a function of effective specific impulse for a perfectly heat-shielded rectangular cross-section contact ionization engine at a current density of 200 amp/m². This theoretical curve is presented for its heuristic value. It is not intended to indicate that the porous tungsten ion engine can be operated now at this level of rocket efficiency.

Conclusion

A moderately efficient porous tungsten ion engine has been operated. Current densities as high as 113 amp/m² have been recorded. Power efficiencies up to 70% have been obtained at a specific impulse of 8680 sec. The ion current intercepted at the accelerating electrode was 5% of the ionizer current for this data point. The explanation as to the exact cause of this relatively high impingement is not available presently as the ion optics of this design are not defined.

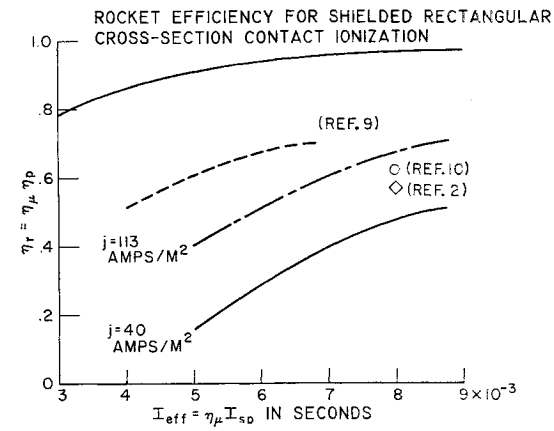

Fig. 8 Comparison of rocket-power efficiencies at various effective specific impulse between the reported contact ionization rocket engines and the electron-bombardment ion-rocket engine

Electron-beam welding shows great promise for ion-rocket application. It leads to a simpler, more compact design, as well as eliminating possible poisoning of the emitter on the blocking of the emitter pores near the ionizer joint by joining materials. One experimental value for propellant-utilization efficiency has been obtained. This value is ≈90% (±3%).

It has been demonstrated that with proper heat shielding and engine design the major sources of power loss from the engine can be reduced. Power inputs of as low as 1.51 × 10⁵ w/m² at an ionizer temperature of 1370°K have been obtained.

References

[1] Staff of the Fluid Physics Division, "Investigation of ionized gases and acceleration systems for ion propulsion," Electro-Optical Systems Final Rept. 150 (July 20, 1960).

[2] Etter, J. E., Eilenberg, S. L., Anderson, J. R., and Ward, J. W., "Recent developments in the production and neutralization of ion beams," ARS Preprint 61-81-1775 (June 1961).

[3] Lockwood, D. L. and Cybulski, R. J., "Performance evaluation of a two-dimensional ion rocket using through-feed and porous tungsten ionizers," NASA TN D-766 (1961).

[4] Keller, T. A., "NASA electric rocket test facilities," Paper R-25, Natl. Sym. Vacuum Technol., Trans. (1960).

[5] Richley, E. A., Sandborn, V. A., Baldwin, L. V., and Dangle, E. E., "Comparative measurements of beam power in ion-rocket research," NASA TN D-845 (1961).

[6] Cybulski, R. J., Kotnik, J. T., and Lockwood, D. L., "Experimental performance of an ion rocket engine using a rectangular slab porous tungsten emitter," NASA TN D-1321 (November 1962).

[7] Mickelsen, W. R., "Application of space charge flow theory to electro-static rocket engine design," NASA TN D-1568 (1963).

[8] Reynolds, T. W. and Kreps, L. W., "Gas flow, emittance, and ion current capabilities of porous tungsten," NASA TN D-871 (1961).

[9] Reader, P. D., "Investigation of a 10-cm-diameter electron-bombardment ion rocket," NASA TN D-1163 (1961).

[10] Ernstene, M. P., Forrester, A. T., James, E. L., Telec, D., and Worlock, R. M., "Development of high efficiency cesium ion engines," ARS Preprint 61-83-1777 (June 1961).